W:Ti Flexible Transversal Electrode Array for Peripheral Nerve Stimulation: A Feasibility Study

Carolina Silveira, *Graduate Student Member, IEEE*, Emma Brunton, *Member, IEEE*, Enrique Escobedo-Cousin, Gaurav Gupta, Roger Whittaker, Anthony O'Neill, *Senior Member, IEEE*, and Kianoush Nazarpour, *Senior Member, IEEE*

***Abstract*— The development of hardware for neural interfacing remains a technical challenge. We introduce a flexible, transversal intraneural tungsten:titanium electrode array for acute studies. We characterize the electrochemical properties of this new combination of tungsten and titanium using cyclic voltammetry and electrochemical impedance spectroscopy. With an *in-vivo* rodent study, we show that the stimulation of peripheral nerves with this electrode array is possible and that more than half of the electrode contacts can yield a stimulation selectivity index of 0.75 or higher at low stimulation currents. This feasibility study paves the way for the development of future cost-effective and easy-to-fabricate neural interfacing electrodes for acute settings, which ultimately can inform the development of technologies that enable bi-directional communication with the human nervous system.**

***Index Terms*— Flexible neural interfaces, peripheral nerve stimulation, selective stimulation.**

I. Introduction

DELIVERING sensory feedback for prosthesis users has attracted a significant level of scientific and clinical interest [1]–[5]. Proof-of-principle demonstrations of closed-loop control of prosthetic limbs are the manifestation of an increasing understanding of the human sensorimotor system and development of appropriate neural interfacing technology [6]–[8]. For instance, using different encoding and nerve stimulation approaches, the information from the sensors, which are typically embedded into prosthetic limbs, can be mapped onto sensations, such as pressure, touch, vibration as well as others, e.g. tingling, as reported by the users [2]–[4], [6]–[11]. However, different groups approach this problem from different angles with marked differences in the site in the nervous system where the stimulation is delivered: central [12]–[14] vs. peripheral nervous system [2], [15]–[17]; invasive [2], [7], [8], [10], [18] vs. non-invasive [5], [17], [19]; and the way the neural stimulation is modulated to convey sensory precepts: biomimetic [8]–[10], [20]–[23] vs. abstract [13], [17], [21], [24]. We believe that this diversity is due to three main reasons: 1. uncertainty on how to best sense and convert sensory information from the environment to electrical patterns to stimulate the nervous system and evoke naturalistic sensation; 2. lack of technologies for targeted delivery of this information to the nervous system; and 3. research still ongoing on the development of biocompatible neural interfaces that allow direct communication with the peripheral nervous system without causing physical damage and pain.

There are different types of neural interfaces, typically divided according to their invasiveness to the tissues and selectivity of stimulation [25]. Within the more invasive category there are well-known electrodes such as the transverse intrafascicular multichannel electrode (TIME) [26], the longitudinal intrafascicular electrode (LIFE) [27], the Utah Slanted Electrode Array (USEA) [28], the 3D spiked ultraflexible neural interface (SUN) [29] and the self-opening neural interface (SELINE) [30]. All of these electrodes allow for a high degree of selectivity and consequently tailored stimulation. These intrafascicular electrodes have been tested in acute and in chronic settings with the purpose of enabling protheses forward control and sensory feedback, reducing phantom limb pain, and helping improve the natural movement of users [3], [10], [15], [31]–[36]. Within the less invasive category of neural interfaces the most common are neural cuffs and the flat interface nerve electrode (FINE), which have also been extensively studied and implanted in patients for decades or in animal models in chronic experiments [25], [37]–[40].

One key characteristic that is highly desirable of neural interfaces is the ability to smoothly adhere or adapt to the biological structures at the implant site, and to conform to the surrounding mechanical conditions [29], [41], [42]. Flexible interfaces have been identified as a solution to reduce this mismatch between the device and the implant medium [43]. As such, there have been advances in the field of flexible interfaces, building upon the traditional and well-established neural cuff. In [44], Xiang *et al.* presented a flexible neural

Manuscript received May 12, 2020; revised July 1, 2020; accepted July 12, 2020. Date of publication August 13, 2020; date of current version October 8, 2020. This work was supported by EPSRC grants under Grant EP/N023080/1, Grant EP/R004242/1, Grant EP/K028421/1, and Grant EP/M025977/1. *(Corresponding author: Kianoush Nazarpour.)*

Carolina Silveira, Emma Brunton, Enrique Escobedo-Cousin, Gaurav Gupta, and Anthony O'Neill are with the School of Engineering, Newcastle University, Newcastle upon Tyne NE1 7RU, U.K.

Roger Whittaker is with the Translational and Clinical Research Institute, Newcastle University, Newcastle upon Tyne NE2 4HH, U.K.

Kianoush Nazarpour is with the School of Engineering, Newcastle University, Newcastle upon Tyne NE1 7RU, U.K., and also with the Biosciences Research Institute, Newcastle University, Newcastle upon Tyne NE2 4HH, U.K. (e-mail: kianoush.nazarpour@newcastle.ac.uk).

Digital Object Identifier 10.1109/TNSRE.2020.3014812

ribbon with coated gold contacts capable of adapting to the shape of peripheral nerves or branches. The neural ribbon was able to selectively record neural signals from the different sciatic nerve branches. The flexible split ring electrode [45], having four gold:platinum (Au:Pt) contacts, also targeted nerve branches or small nerves and achieved selective stimulation of different muscles by varying the configuration of the active stimulating contacts. In [45], Lee *et al.* also presented a flexible neural clip with coated iridium oxide contacts that focused on showing the importance of flexible designs to better adapt to nerve structures. Therefore, it is clear that flexibility has been and will continue to be a sought-after characteristic for neural interfaces [42], [43], [46]. From the most invasive group of interfaces the TIME electrode is the flexible interface that has been more widely used and reported high selectivity of stimulation [26], [47]. The TIME electrode used in acute studies is comprised of 10 platinum-black circular active sites of 60 μm in diameter.

Another key factor to take into account in a neural interface is the material of the electrode contacts. The most crucial requirements of these materials include minimal tissue response, low impedance in contact with the tissue, enough charge storage capacity and they should not corrode or delaminate [48], [49]. Numerous materials have been used over the years and some of the most popular are platinum, platinum:iridium, gold, titanium nitride and tungsten [25], [48], [50]. More recently, some of the new emerging materials are PEDOT:PSS, carbon nanotubes [50], ruthenium oxide [51] and conductive elastomers composites [52]. Considering more traditional materials, tungsten has been described as a valuable material for neural signal recording [25], [48], [49], however, it has not been comprehensively investigated for its stimulation capabilities. Tungsten is a good candidate for acute laboratory studies as it is an easy material to deposit on a parylene-C substrate; its flexibility can be improved by conjugation with other metals, and it is a cheaper than platinum.

The aim of this article is to report our progress on the use of a flexible intraneural tungsten:titanium (W:Ti) electrode array for stimulation of peripheral nerves. In this feasibility study, we acutely implanted the fabricated electrode array in the sciatic nerve of four rats aiming to answer two questions: 1) Can the flexible electrode stimulate peripheral nerves? and 2) Can the stimulation be selective?

To address these questions, electroneurographic (ENG) signals were recorded from the two main sciatic nerve branches (tibial and peroneal) and electromyographic (EMG) signals recorded from the Gastrocnemius (GM) and Tibialis Anterior (TA) muscles, both of which are innervated by the sciatic nerve branches. The threshold and maximum stimulation current of each electrode contact were identified by visually observing the EMG signal response on an oscilloscope. Selectivity of stimulation was assessed by analysing the peak-to-peak amplitude of the compound muscle action potentials (CMAP) and calculation of a selectivity index (SI). For completeness, electrochemical characterisation of the electrode array was carried out by running cyclic voltammetry (CV) and electrochemical impedance spectroscopy (EIS).

II. Methods

A. Design and Fabrication of the Flexible Electrode Array

The flexible electrode array comprises twenty four recording/stimulating sites sandwiched between two 10 μm-thick layers of parylene-C. The metallisation for the active sites and connecting tracks uses a tungsten:titanium ($W_{0.8}Ti_{0.2}$) alloy to provide greater flexibility compared to using tungsten alone. The fabrication process is summarised in figure 1. The electrode arrays were fabricated on 3-inch silicon wafers using standard semiconductor processing techniques. Each recording site has a rectangular shape with rounded corners, width of 25 μm, length of either 50 or 75 μm, and a separation of either 50 or 75 μm. The electrodes were connected to a bond-pad via W:Ti tracks, and the bond-pads connect to a matching, custom-made PCB to interface with the stimulation system.

The silicon wafer is solvent-cleaned in N-Methyl-2-pyrrolidone (NMP) and isopropanol (IPA) to remove organic contamination. The 300 *n*m-thick sacrificial aluminium layer is deposited on the silicon surface by sputtering in an Oxford Instruments Plasmalab 400 DC & RF system, at a process pressure of 10 mTorr. The first layer of parylene-C is deposited to a thickness of 10 μm in a SCS Labcoater™(PDS 2010). Next, a 1 μm-thick film of W:Ti is deposited by magnetron sputtering in the Oxford Instruments Plasmalab sputtering system from a 99.9% pure W:Ti target from Pi-Kem. The chamber environment was maintained at a pressure of 19 mTorr by a constant Ar gas flow of 15 sccm. The DC power used was 100 W. The W:Ti was then patterned by reactive ion etching (RIE) in a Plasma-Therm 790 machine, at a pressure of 150 mTorr and power of 175 W, using AZ 5214E photoresist from MicroChemicals as a mask. The gas mixture in the chamber was SF6 (40%)/Ar (60%). The etch rate for W:Ti under these parameters is 200 *n*m/min. Following RIE etching, the photoresist mask can be removed using NMP and IPA. The patterned W:Ti is then capped with a second parylene-C layer of 10 μm. A 30 *n*m-thick titanium mask is outlined on top of the parylene-C surface in order to pattern the final probes. The Ti mask is deposited by e-beam and patterned by direct photo-lithography. Dry etching of the parylene-C was carried out in oxygen plasma in a custom-made etcher system by Oxford Instruments. The gas mixture in the chamber was O_2 only. Following parylene-C etching, the remaining Ti mask is removed in H_2O:HF (30:1) for 5-10 s. Finally, the probes are released from the carrier by dissolving the sacrificial aluminium layer in tetramethylammonium hydroxide at 60° C.

B. Electrochemical Characterization

The CV and EIS methods were performed using Autolab PGSTAT302N. A three-electrode configuration set-up in PBS (pH 7.4, Gibco™) was used for these measurements. The counter electrode was a high surface area platinum mesh; the non-current carrying reference was an Ag|AgCl leakless electrode (eDAQ ET069-1) and the working electrode was the flexible electrode contact under test. A potential range of −1 to 1 V vs. Ag|AgCl was used to generate the CV curve at a sweep rate of 50 mV/s. EIS was run at 0.1 V vs.

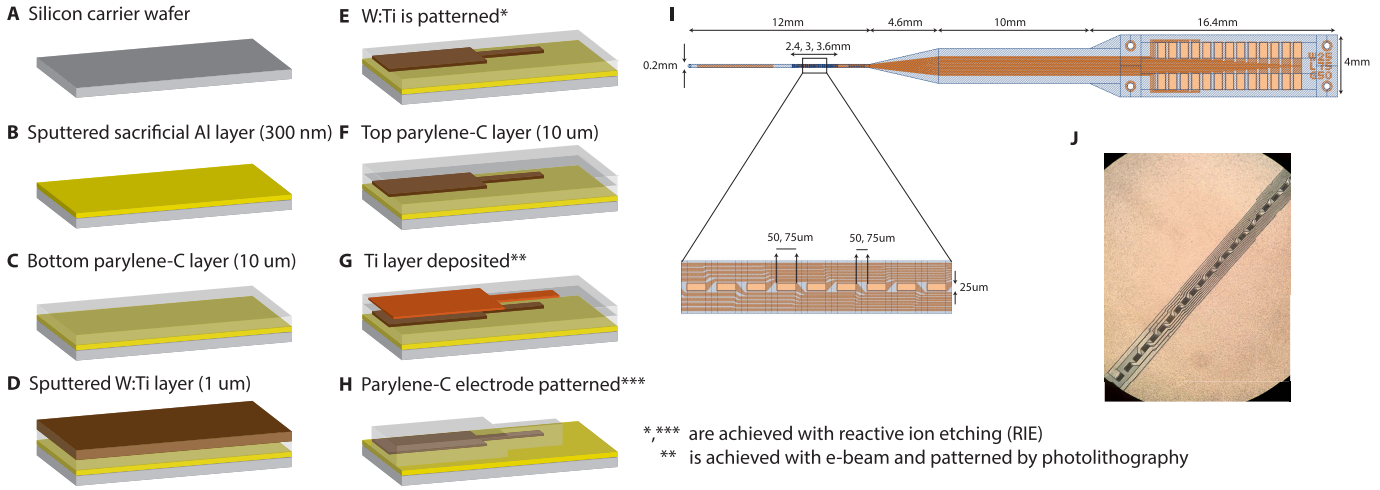

Fig. 1. A-H: Summary of the fabrication process of the flexible electrodes; I: Dimensions of the fabricated electrode. The zoomed window shows the actual electrode contacts which are either 50 or 75 μm in length and have a gap of either 50 or 75 μm. The length of the recording area is either 2.4 mm, 3 mm or 3.6 mm; J: A microscopic image of the electrode.

Ag|AgCl between 10 Hz to 100 kHz at an amplitude of 10 mV. This potential was chosen for running the EIS since it was within the range where no irreversible reactions happen for this electrode.

C. Animal Preparation and Surgery

All animal care and procedures were approved by UK Home office under the Animals (Scientific Procedures) Act (1986) and by the Animal Welfare and Ethical Review Board of Newcastle University. Animals were housed in a 12 hour light/dark cycle with food and water available *ad-libitum*. Four Sprague-Dawley rats weighing 300-400 g were acutely implanted with the electrode in the sciatic nerve. A total of five experimental sessions (sessions 0-4) were conducted in four consecutive days. Sessions 3 and 4 were carried out on the same day and with same animal.

For induction of anaesthesia the animals were placed inside a box of 3% isoflurane in oxygen. A meloxicam injection (1 mg/kg) was administered and isoflurane in oxygen was delivered through a nose mask. The isoflurane levels were constantly adjusted throughout the experiment for maintaining depth of anaesthesia. The heart rate and oxygen saturation levels were monitored with the help of a pulse oximeter. A tail vein cannula was used to deliver 20 ml of saline (0.9% NaCl and 5% glucose) with 0.05 ml of KCL to keep fluids and hydration levels. The animal was placed on the surgical table on top of a heat-pad with a skin temperature probe. The surface temperature was kept between 36-37° C.

A skin incision was made at approximately 0.5 cm caudal and parallel to the femur and the gluteus superficialis and biceps femoris muscles were blunt dissected. The sciatic nerve trunk and its peroneal and tibial branches were exposed, separated and cleared from fat and connective tissue. The TA and the GM muscles were also exposed through skin incisions. A tungsten ground wire was attached to the L5 spinous process using dental acrylic after clearing it from the surrounding muscles and connective tissue.

Finally, an overdose of pentobarbital was administered and confirmation of death was assessed by cessation of circulation and onset of *rigor-mortis*. Further details about the surgical process can be found in [16], [18], [53].

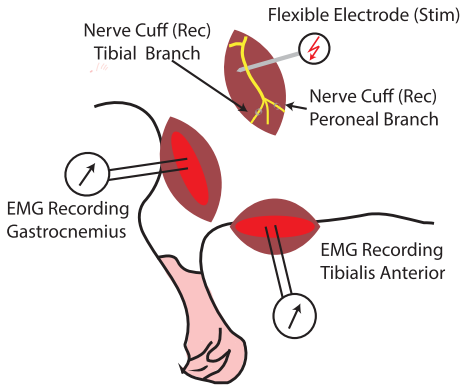

Fig. 2. The experimental set-up. Neural stimulation was delivered through the flexible electrode implanted in the sciatic nerve trunk. The ENG signals were recorded from the tibial and peroneal branches of the sciatic nerve, distal to the bifurcation site using in house built micro half-cuffs. The EMG signals were recorded from the GM and TA muscles.

D. Placement of Stimulation and Recording Electrodes

The flexible electrode array does not have the mechanical strength to penetrate the sciatic nerve. Therefore, it was implanted with the help of a micro-needle. Under a microscope, the needle was put through the main branch of the sciatic nerve and the electrode array was threaded into the needle. The needle was then removed, leaving the electrode implanted in the nerve. The electrode was held in place with the help of a magnetic stand holding on to the PCB connector.

The experimental set-up is shown in figure 2. Two micro half-cuffs were placed on the peroneal and tibial branches of the sciatic nerve. The half-cuffs were 3D printed in-house and were used to record neural responses from the tibial and peroneal nerve branches. The cuffs had a rectangular shape and measure 3.5 by 2 by 2 mm. They were designed with two small side-holes (0.65 mm in diameter) through which two tungsten wires were threaded for bipolar recording.

The EMG signals of the TA and GM muscles were recorded using two intramuscular tungsten wire electrodes. These wires

were fixed in position using tissue glue and the skin surrounding the electrodes was glued together, using tissue glue as well. During the first experimental session (session 0) only the TA EMG signals were recorded. In experimental sessions 1-4 the EMG was recorded from both the TA and GM muscles.

E. Stimulation and Recording Systems

Stimulation was delivered with a CereStim R96 (Blackrock Microsystems, USA) in four out of five experimental sessions (sessions 0–3). The stimulation ground electrode, a stainless steel wire, was positioned in the skin close to the flexible electrode. The PCB board of the flexible electrode was connected to the CereStim using the CereStim R96 cable (Samtec MIT-019-02-F-D). The EMG recording wires and the ENG recording half-cuffs were connected to a differential amplifier (A-M Systems™, USA) and bandpass filtered between 10 Hz-1 kHz and between 10 Hz-5 kHz, respectively. The outputs of the amplifier were connected to the analog inputs of a Cerebus Neural Signal Processor (Blackrock Microsystems, USA) where both the compound action potentials (CAP) from the nerve branches and the CMAP were sampled at 30 kHz.

On the last experiment day, a second round of stimulation was performed (session 4) using an isolated pulse stimulator (model 2100, A-M Systems™, USA). The AM-Systems allowed for stimulating with shorter pulse widths. Experimental sessions 3 and 4 were carried out consecutively on the same animal and using the same electrode array. However, in between sessions 3 and 4 the electrode array was removed, checked for continuity and reimplanted.

F. Stimulation Protocol

The diameter of the rat sciatic nerve measures approximately 1-1.5 mm [54]. Due to the size of the contacts and inter-electrode pitch, not all of the 24 active sites can be in contact with the tissue following implantation. Therefore, the electrodes in contact with the nerve were identified by measuring their impedances at 1 kHz using the CereStim. Half way through the experimental session the electrode was moved along the nerve so that the contacts that sit in the opposite end of the electrode could also be implanted in the nerve. We decided to take this approach because understanding the relationship between the contacts' position in the nerve and the selectivity of stimulation was outside the remit of this feasibility study.

The threshold and maximum stimulation currents were identified by visually monitoring the EMG signal activity on the oscilloscope. To find these values the starting current level was 50 μA and it was increased/ decreased in steps of 5 μA and 1 μA. The CMAP signals were observed for both muscles simultaneously and as soon as activity was detected in one muscle the current level was noted as the stimulation threshold for that electrode contact. Once the threshold was found, the stimuli were delivered 10 times via the electrode contact with a pause of 0.5 s between each stimulation pulse. This process was repeated for all the electrode contacts that were functional. The maximum stimulation current of each electrode contact was found by progressively increasing the current level and observing when the CMAP signal on either muscle would cap. Stimuli were then delivered ten times at 100%, 80%, 60%, 40%, 20% of the maximum current value. The difference between the maximum and threshold currents was calculated and referred to as the dynamic range.

The stimulation parameters used with the CereStim were symmetric biphasic cathodic-first pulses of 50 μs pulse width and 53 μs inter-pulse delay at 1 Hz. In session 4, an AM-systems stimulator was used to investigate the effect using a monophasic cathodic 40 μs pulses at 1 Hz.

G. Data Analysis

The ENG and EMG signals were normalised to baseline and averaged over the ten stimuli collected for each threshold and each percentage of the maximum stimulation value. The peak-to-peak values of the EMG CMAPs were the features extracted to estimate muscle activity. The ENG signals were analysed between 0.5 ms and 1.5 ms to include the CAP and exclude the artefact, which happened before 0.5 ms. The distance between the flexible electrode (stimulating electrode) and the EMG recording wires was approximately 2-3 cm. Given the nerve conduction velocity (60 $\frac{m}{s}$ and the neuromuscular junction delay, we did not expect an M-wave before 2 ms [55]. Hence, we analysed the EMG signals between 2-8 ms.

The peroneal branch of the sciatic nerve innervates the TA muscle, whereas the GM muscle is innervated by the tibial branch [47]. Thus, the activation of the TA and GM muscles were used to investigate whether the fabricated electrode can achieve selective stimulation of the branches and the associated muscles. The peak-to-peak amplitude of the CMAP (M-wave) was normalized to the maximum peak-to-peak CMAP amplitude obtained for each muscle as measured at 100% of maximum stimulation. We use the flexible electrode for this and found the overall maximum of each muscle in each experimental session. For each contact that was verified to be in contact with the tissue i, a selectivity index ($SI_{i,k}$) was estimated as the ratio between the normalized CMAP peak-to-peak amplitude of the muscle of interest, and the sum of the normalized CMAP peak-to-peak amplitudes evoked in both GM and TA muscles [56]:

$$SI_{i,k} = \frac{CMAP_{i,k}}{\sum_j CMAP_{i,j}}.$$

The SIs were calculated at threshold and at four of the five stimulation levels (40%, 60%, 80% and 100% of maximum stimulation) for both the TA and GM muscles. A SI of 0.75 was chosen as the minimum index value to consider that selective stimulation was achieved.

III. Results

A. Electrochemical and Functional Characterisation of the Electrode Array

Figure 3A,B shows the results of the electrochemical characterisation of the electrode array in PBS solution (pH 7.4, Gibco ™) using CV (−1 V to 1 V) and EIS for two contacts of the electrode array. These contacts presented similar behaviour in both their CV and EIS curves. The two peaks observed in CV (figure 3A) around −0.5 V and 0.6 V indicate the water window limits for this tungsten:titanium alloy. The peaks

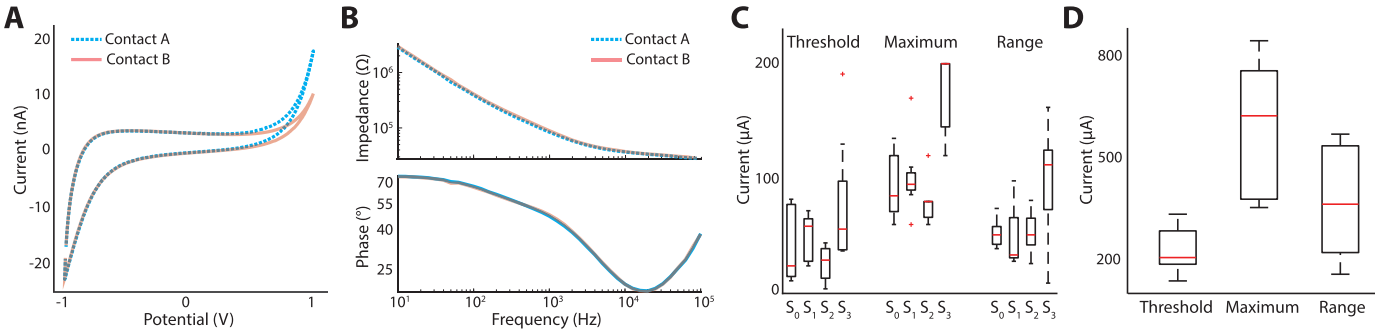

Fig. 3. Electrochemical and functional characterisation of the electrode array; A: Cyclic voltammetry of two contacts of the flexible electrode. The CV was run between −1 V and 1 V at a sweep rate of 50 mV/s. Three CV sweeps were run and the third run is shown; B: Impedance magnitude and phase of the EIS done on the two electrode contacts. The frequency range used was 10 Hz to 100 kHz at a potential of 0.1 V; C: The thresholds, maximum and dynamic range of stimulation of four experimental sessions ($S_0 - S_3$); and D: Thresholds, maximum and dynamic range of stimulation when using the AM system stimulator (session 4). In the boxplots the red mark is the median, the edges represent the 25th and 75th percentiles, the whiskers extend to the most extreme data points the algorithm does not consider to be outliers, and the outliers are plotted in red.

seen in the CV curve represent the moment when irreversible reactions, such as oxidation and reduction of oxygen, start to take place and thus the potential of 0.1 V was chosen for the EIS as this lies in the region where no irreversible reactions take place. The EIS results showed a capacitive curve with a decrease of phase angle with decreasing frequency. At 1 kHz the impedance magnitude was approximately 89 kΩ, which falls in the range of 50 kΩ to 1 MΩ impedance for *in vivo* studies as reported in [50].

The thresholds for triggering muscle activation as well as the maximum of stimulation were found for each working contact of the electrode. This was carried out by visual observation of the EMG response on the oscilloscope. Figure 3C shows the thresholds, maximum and dynamic range of stimulation of the four experimental sessions done using the CereStim stimulator (sessions 0-3). The additional results obtained on session 4 with the AM-systems stimulator are shown in figure 3D. In comparison, the currents obtained in sessions 0-3 were highly variable ranging from 4 to 191 μA (thresholds) and from 60 to 200 μA (maximum), whereas the results obtained with the AM-systems stimulator in session 4 ranged from 130 to 330 μA (thresholds) and from 350 to 850 μA (maximum).

B. Selectivity of Stimulation

Figure 4 shows an example of the EMG and ENG traces obtained when stimulating with one of the flexible electrode contacts. The shown traces are the average of the 10 stimulation pulses delivered for each percentage of the maximum and are normalised to the baseline. Part A of this figure shows the GM muscle traces (top) and the TA muscle (bottom) while part B shows the corresponding Tibial branch (top) and the Peroneal nerve branch (bottom) neural recordings.

In figure 4B the grey shade covers the first 0.5 ms of the recorded signals which contains the stimulation artefact. The CAP can only be seen after this. The peak-to-peak amplitude of the TA muscle response is smaller compared to the amplitude of the GM muscle. Therefore, figure 4 is an example where selectivity of stimulation can be observed in the raw data for the GM muscle at stimulation currents corresponding to 80% and 100% of the maximum current.

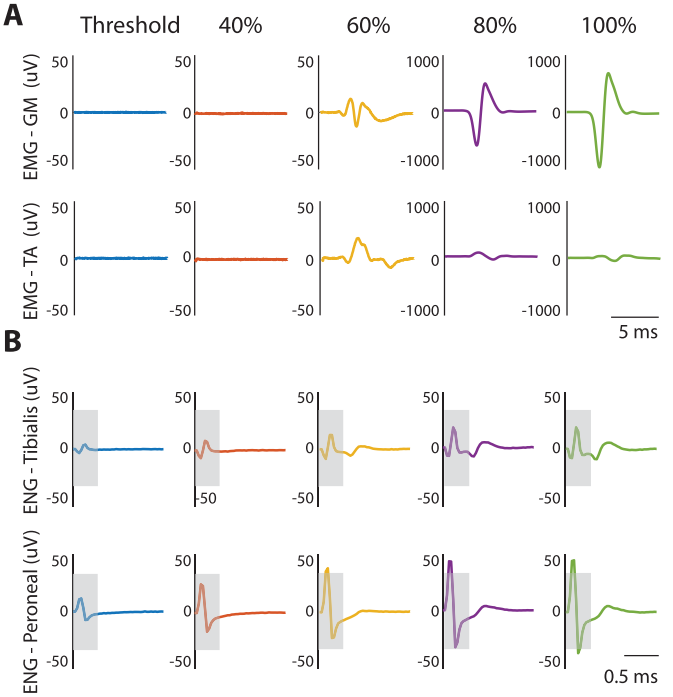

Fig. 4. Example of recorded EMG and ENG waveforms showing selective stimulation of the GM muscle. The traces are for threshold, and 40%-100% of the maximum stimulation level.

Figure 5A quantifies the selectivity of stimulation of the sciatic nerve, and consequently the GM and TA muscles, using the fabricated electrode array. For clarity, in figure 5A, the results are shown at threshold and at 100% of maximum stimulation for each contact. The results of experiment sessions 1 and 2 show clear selectivity for the TA muscle at threshold which expectedly disappears at 100% of maximum stimulation. In session 3, the TA muscle also showed selectivity at threshold (SI $>$ 0.75) for all the contacts but at 100% of maximum 4 out of 9 contacts could selectively stimulate the TA muscle and 1 out of 9 contacts the GM muscle. The results of session 4 show that different contacts of the same electrode can provide selective stimulation of different muscles. Specifically, two contacts show selectivity at threshold for the TA muscle while four contacts show selectivity at threshold for the GM muscle. However, at maximum stimulation two

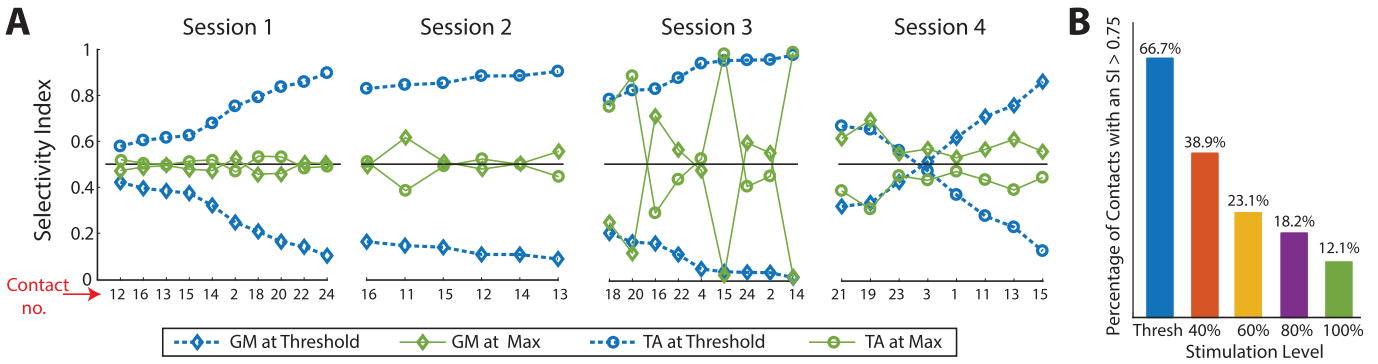

Fig. 5. Selectivity Analysis. A: Selectivity indices of the GM and TA muscles at threshold and at maximum of stimulation (Max) in experiment sessions 1-4. The EMG recordings were only collected from two muscles, thus the selectivity indexes are complementary, adding up to 1. The x axis denotes the contact ID of the electrode arrays and the y axis the selectivity index. A total of 3 electrode arrays were used in sessions 1-4 since the same electrode was used in sessions 3 and 4. B: Percentage of contacts, across sessions 1-4, with a selectively index higher than 0.75. The contacts with threshold currents higher than the current levels at 40% and 60% of maximum stimulation were not included in this graph.

contacts provided selective stimulation of the GM muscle, while at threshold the same two contacts had been able to selectively stimulate the TA muscle. The results of session 4 also show, however, that there is a less pronounced gap between selectivity achieved at threshold and at maximum of stimulation.

Finally, figure 5B summarises the percentage of contacts across experiment sessions 1-4 that resulted in a SI of at least 0.75. Expectedly, the graph shows that with increasing stimulation levels less contacts were able to selectively recruit either one of the muscles. In this graph the results of the 20% of maximum stimulation current were not included because in 91% of the cases these values were lower than the threshold of the stimulation current. Therefore, for those cases, the stimulation current was not high enough to evoke any discernible EMG signals. The same happened for 15 out of the 33 electrode contacts at 40% of maximum stimulation and for 7 (out of 33) contacts at 60% of maximum stimulation. Thus, these contacts were not included in figure 5B.

IV. Concluding Remarks

In this study, an in-house fabricated flexible electrode array was acutely implanted in the sciatic nerve of rats to understand if this electrode recipe could stimulate the nerve and if this stimulation could be selective. Results showed that stimulation was possible and at threshold 67% of the contacts achieved a SI of 0.75 or higher for recruitment of either the GM or TA muscles. The EMG signals were only recorded from two muscles, thus a SI of 0.5 does not indicate selectivity. An SI of 0.75 was therefore chosen as the minimum index of selectivity. An SI of 0.75 does not necessarily mean that high selectivity was achieved but instead shows that the stimulation was selective.

At 40% of maximum stimulation 39% of the contacts also achieved a SI of at least 0.75 because for those contacts the current levels were close to the threshold levels. In contrast, at maximum stimulation current only 12.1% of contacts had SIs higher than 0.75. As expected, and reported in other studies with the intrafascicular TIME electrode, the higher the stimulation current the lower the selectivity due to the spread of current to neighbouring nerve fascicles that innervate other muscles [26], [47]. For the selectivity analysis, the contacts that at 40% and 60% of stimulation did not reach the threshold current level were not included since they would have not triggered a muscle response. In these cases, the dynamic range was low and for that reason even at 60% of maximum stimulation the threshold of activation had not been reached.

The results of sessions 3 and 4 also showed that for 8 out of 17 contacts a similar SI was found at both threshold and maximum of stimulation. It may indicate that those contacts were able to more specifically target fascicle bundles. This could also be because of the mentioned low dynamic range where the proximity in value of the threshold and maximum current could allow for similar selectivity of stimulation. It is important to highlight that sessions 3 and 4 were performed with the same electrode array - only the stimulator and parameters of stimulation were different. Furthermore, the positioning of the electrode and therefore the contacts that were inside the nerve changed between session 3 and session 4 as the electrode array was re-implanted when switching stimulators. We believe this is what probably allowed for recruiting different muscles with the two different stimulators. The different waveform parameters are likely to have played a role in the threshold and maximum current value differences observed between session 4 and the other sessions. Future work is required to understand the impact of the waveform parameters on the stimulation selectivity.

The current thresholds for muscle activation of sessions 0-3 varied between 3 μA and 130 μA except for one outlier at 191 μA. These values are higher than what was reported with other intraneural electrodes (20 to 100 μA with the TIME [26] and 24 to 66 μA with TIME and LIFE devices [47]). This could be due to a poorer contact at the electrode-tissue interface caused the by the inherent damage of passing a 200+ μm wide needle through the nerve or due to the different metals' combinations used for stimulation. Furthermore, since we only recorded from two muscles, the thresholds of some contacts might appear higher for the TA or the GM muscle because their position in the nerve would better target a different subset of fibres innervating muscles we did not record from.

We chose the peak-to-peak amplitude of the CMAP as the parameter to analyse the EMG signals. The area under the

curve was also extracted from the signals and the results in terms of selectivity of stimulation were equivalent to the peak-to-peak results. The same analysis was performed for the ENG signals. We did not observe ENG selectivity as we showed in the EMG domain. We believe that it was because the recorded ENG signals were not always able to capture the action potentials even though the CMAPs were captured. Perhaps this could be due to the suboptimal contact between the recording 3D-printed cuffs and the nerve; the nerve branches sat on the cuff wires partially.

For the development of flexible electrode array, parylene-C was the polymer of choice for the substrate given its adherence properties, inertness and deposition technology at room temperature [41]. The mechanical, dielectric and barrier properties of parylene-C are comparable to those of other commonly used polymers such as polyimide. However, the deposition of most polymers requires them to be spun on the sample as a liquid and liquid-phase deposition can lead to bubble formation. In addition, surface tension prevents the polymer to fill micron-size features effectively, which can lead to encapsulation failure. In contrast, parylene-C can be deposited as a vapour, resulting in bubble free, air-tight, conformal layers. Furthermore, the parylene-C layer thickness can be accurately controlled to sub-micron resolutions, which improves reproducibility in the fabrication process [57]. However, using polyimide instead of parylene-C as the substrate could be beneficial for the chronic stability of intraneural implants [57], [58]. Oliva *et al.* looked at the fibrotic response of parylene-C based intraneural implants in rats over a period of more than six months and found the response larger than that of polyimide. In addition, the lifetime of parylene-C encapsulated implants is shorter than previously estimated [59]. Therefore, polyimide could be a more adequate substrate for chronic neural implants while parylene-C remains an adequate material for acute applications.

Tungsten electrodes have been used for more than 60 years to record from the central nervous system in chronic settings [60]–[63]. To our knowledge, the potential of tungsten:titanium electrode for the stimulation of the peripheral nerves has not been studied. It can be useful, in acute settings, to experiment with different material combinations and configurations to better understand how these influence stimulation. The electrodes still need to be non-toxic and sufficiently robust to survive several tissue insertions. Tungsten and gold are readily compatible with microfabrication techniques as they can be deposited either by evaporation or sputtering. Platinum deposition occurs at high energy, which may lead to thermal stress and cracking of the underlying parylene-C. Gold and tungsten can be evaporated on parylene-C without causing damage, however, gold has extremely poor adhesion to parylene-C which may result in a 50% reduction of yield compared to tungsten. We sought to determine if it would be feasible to use a tungsten:titanium alloy for the electrode surfaces and interconnecting tracks ($W_{0.8}Ti_{0.2}$ ratio) to provide greater flexibility, as the Young's modulus of W:Ti is 110 GPa, compared with 400 GPa, for tungsten alone [64].

Future work on the presented flexible electrode array will include reducing its overall dimensions to better fit the sciatic nerve of rats. The number of available stimulating and recording contacts can also be reduced since with the transversal implantation not all of the 24 contacts fit within the nerve. Before chronic studies can be conducted with the flexible electrode more rounds of design improvement and therefore acute studies are necessary. Incorporating an anchoring mechanism to keep the electrode in place and changing the substrate to polyimide are examples of improvements. With the current fabrication method different electrode designs (e.g. contact size, shape or separation) can be made on the same wafer, allowing for a direct comparison of the outcome. Experimenting with different conventional metals and combinations of metals is also an alternative to find a good balance between cost, ease of fabrication and functionality.

REFERENCES

[1] G. S. Dhillon and K. W. Horch, "Direct neural sensory feedback and control of a prosthetic arm," *IEEE Trans. Neural Syst. Rehabil. Eng.*, vol. 13, no. 4, pp. 468–472, Dec. 2005.

[2] D. W. Tan, M. A. Schiefer, M. W. Keith, J. R. Anderson, J. Tyler, and D. J. Tyler, "A neural interface provides long-term stable natural touch perception," *Sci. Transl. Med.*, vol. 6, no. 257, p. 257ra138, 2014.

[3] H. A. C. Wark, K. S. Mathews, R. A. Normann, and E. Fernandez, "Behavioral and cellular consequences of high-electrode count utah arrays chronically implanted in rat sciatic nerve," *J. Neural Eng.*, vol. 11, no. 4, Aug. 2014, Art. no. 046027.

[4] G. Di Pino *et al.*, "Invasive neural interfaces: The perspective of the surgeon," *J. Surgical Res.*, vol. 188, no. 1, pp. 77–87, May 2014.

[5] J. Dong *et al.*, "The variability of psychophysical parameters following surface and subdermal stimulation: A multiday study in amputees," *IEEE Trans. Neural Syst. Rehabil. Eng.*, vol. 28, no. 1, pp. 174–180, Jan. 2020.

[6] K. Horch, S. Meek, T. G. Taylor, and D. T. Hutchinson, "Object discrimination with an artificial hand using electrical stimulation of peripheral tactile and proprioceptive pathways with intrafascicular electrodes," *IEEE Trans. Neural Syst. Rehabil. Eng.*, vol. 19, no. 5, pp. 483–489, Oct. 2011.

[7] M. Ortiz-Catalan, B. Håkansson, and R. Brånemark, "An osseointegrated human-machine gateway for long-term sensory feedback and motor control of artificial limbs," *Sci. Transl. Med.*, vol. 6, no. 257, p. 257, Oct. 2014.

[8] E. L. Graczyk, M. A. Schiefer, H. P. Saal, B. P. Delhaye, S. J. Bensmaia, and D. J. Tyler, "The neural basis of perceived intensity in natural and artificial touch," *Sci. Transl. Med.*, vol. 8, p. 362, Oct. 2016.

[9] C. M. Oddo *et al.*, "Intraneural stimulation elicits discrimination of textural features by artificial fingertip in intact and amputee humans," *Life*, vol. 5, Mar. 2016, Art. no. e09148,

[10] E. D'Anna *et al.*, "A closed-loop hand prosthesis with simultaneous intraneural tactile and position feedback," *Sci. Robot.*, vol. 4, no. 27, Feb. 2019, Art. no. eaau8892.

[11] M. A. O'Doherty *et al.*, "Active tactile exploration," *Nature*, vol. 479, no. 7372, pp. 228–231, 2012.

[12] B. M. London, L. R. Jordan, C. R. Jackson, and L. E. Miller, "Electrical stimulation of the proprioceptive cortex (Area 3a) used to instruct a behaving monkey," *IEEE Trans. Neural Syst. Rehabil. Eng.*, vol. 16, no. 1, pp. 32–36, Feb. 2008.

[13] D. J. Weber *et al.*, "Limb-state information encoded by peripheral and central somatosensory neurons: Implications for an afferent interface," *IEEE Trans. Neural Syst. Rehabil. Eng.*, vol. 19, no. 5, pp. 501–513, Oct. 2011.

[14] D. A. Bjanes and C. T. Moritz, "A robust encoding scheme for delivering artificial sensory information via direct brain stimulation," *IEEE Trans. Neural Syst. Rehabil. Eng.*, vol. 27, no. 10, pp. 1994–2004, Oct. 2019.

[15] S. Raspopovic *et al.*, "Restoring natural sensory feedback in real-time bidirectional hand prostheses," *Sci. Transl. Med.*, vol. 6, no. 222, pp. 219–222, 2014.

[16] E. Brunton, C. Silveira, J. Rosenberg, M. Schiefer, J. Riddell, and K. Nazarpour, "Temporal modulation of the response of sensory fibers to paired-pulse stimulation," *IEEE Trans. Neural Syst. Rehabil. Eng.*, vol. 27, no. 9, pp. 1676–1683, Jun. 2019.

[17] T. Pistohl, D. Joshi, G. Ganesh, A. Jackson, and K. Nazarpour, "Artificial proprioceptive feedback for myoelectric control," *IEEE Trans. Neural Syst. Rehabil. Eng.*, vol. 23, no. 3, pp. 498–507, May 2015.

[18] C. Silveira, E. Brunton, S. Spendiff, and K. Nazarpour, "Influence of nerve cuff channel count and implantation site on the separability of afferent ENG," *J. Neural Eng.*, vol. 15, no. 4, 2018, Art. no. 046004.

[19] L. Seminara *et al.*, "Dual-parameter modulation improves stimulus localization in multichannel electrotactile stimulation," *IEEE Trans. Haptics*, vol. 13, no. 2, pp. 393–403, Apr./Jun. 2019.

[20] I. Williams and T. G. Constandinou, "An energy-efficient, dynamic voltage scaling neural stimulator for a proprioceptive prosthesis," *IEEE Trans. Biomed. Circuits Syst.*, vol. 7, no. 2, pp. 129–139, Apr. 2013.

[21] T. A. Kuiken, P. D. Marasco, B. A. Lock, R. N. Harden, and J. P. Dewald, "Redirection of cutaneous sensation from the hand to the chest skin of human amputees with targeted reinnervation," *Proc. Nat. Acad. Sci. USA*, vol. 104, no. 50, pp. 20061–20066, 2007.

[22] I. Williams *et al.*, "SenseBack – implant considerations for an implantable neural stimulation and recording device," in *Proc. IEEE Biomed. Circuits Syst. Conf. (BioCAS)*, Oct. 2019, pp. 1–4.

[23] D. Blana *et al.*, "Model-based control of individual finger movements for prosthetic hand function," *IEEE Trans. Neural Syst. Rehabil. Eng.*, vol. 28, no. 3, pp. 612–620, 2020.

[24] H. J. B. Witteveen, F. Luft, J. S. Rietman, and P. H. Veltink, "Stiffness feedback for myoelectric forearm prostheses using vibrotactile stimulation," *IEEE Trans. Neural Syst. Rehabil. Eng.*, vol. 22, no. 1, pp. 53–61, Jan. 2014.

[25] X. Navarro, T. B. Krueger, N. Lago, S. Micera, T. Stieglitz, and P. Dario, "A critical review of interfaces with the peripheral nervous system for the control of neuroprostheses and hybrid bionic systems," *J. Peripheral Nervous Syst.*, vol. 10, no. 3, pp. 229–258, Sep. 2005.

[26] T. Boretius *et al.*, "A transverse intrafascicular multichannel electrode (TIME) to interface with the peripheral nerve," *Biosensors Bioelectron.*, vol. 26, no. 1, pp. 62–69, Sep. 2010.

[27] S. M. Lawrence, G. S. Dhillon, and K. W. Horch, "Fabrication and characteristics of an implantable, polymer-based, intrafascicular electrode," *J. Neurosci. Methods*, vol. 131, nos. 1–2, pp. 9–26, Dec. 2003.

[28] A. Branner and R. A. Normann, "A multielectrode array for intrafascicular recording and stimulation in sciatic nerve of cats," *Brain Res. Bull.*, vol. 51, no. 4, pp. 293–306, Mar. 2000.

[29] J. Wang *et al.*, "A highly selective 3D spiked ultraflexible neural (SUN) interface for decoding peripheral nerve sensory information," *Adv. Healthcare Mater.*, vol. 7, no. 5, pp. 1–8, 2018.

[30] A. Cutrone *et al.*, "A three-dimensional self-opening intraneural peripheral interface (SELINE)," *J. Neural Eng.*, vol. 12, no. 1, Feb. 2015, Art. no. 016016.

[31] I. Strauss *et al.*, "Characterization of multi-channel intraneural stimulation in transradial amputees," *Sci. Rep.*, vol. 9, no. 1, Dec. 2019, Art. no. 19258.

[32] T. S. Davis *et al.*, "Restoring motor control and sensory feedback in people with upper extremity amputations using arrays of 96 microelectrodes implanted in the median and ulnar nerves," *J. Neural Eng.*, vol. 13, no. 3, Jun. 2016, Art. no. 036001.

[33] F. M. Petrini *et al.*, "Sensory feedback restoration in leg amputees improves walking speed, metabolic cost and phantom pain," *Nature Med.*, vol. 25, no. 9, pp. 1356–1363, Sep. 2019.

[34] S. Wendelken *et al.*, "Restoration of motor control and proprioceptive and cutaneous sensation in humans with prior upper-limb amputation via multiple utah slanted electrode arrays (USEAs) implanted in residual peripheral arm nerves," *J. Neuroeng. Rehabil.*, vol. 14, no. 1, p. 14, Dec. 2017.

[35] J. A. George *et al.*, "Biomimetic sensory feedback through peripheral nerve stimulation improves dexterous use of a bionic hand," *Sci. Robot.*, vol. 4, no. 32, Jul. 2019, Art. no. eaax2352.

[36] A. K. Thota *et al.*, "A system and method to interface with multiple groups of axons in several fascicles of peripheral nerves," *J. Neurosci. Methods*, vol. 244, pp. 78–84, Apr. 2015.

[37] D. J. Tyler and D. M. Durand, "Chronic response of the rat sciatic nerve to the flat interface nerve electrode," *Ann. Biomed. Eng.*, vol. 31, no. 6, pp. 633–642, Jun. 2003.

[38] K. H. Polasek, H. A. Hoyen, M. W. Keith, and D. J. Tyler, "Human Nerve Stimulation Thresholds and Selectivity Using a Multi-contact Nerve Cuff Electrode," *IEEE Trans. Neural Syst. Rehabil. Eng.*, vol. 15, no. 1, pp. 76–82, Mar. 2007.

[39] B. P. Christie *et al.*, "Long-term stability of stimulating spiral nerve cuff electrodes on human peripheral nerves," *J. Neuroeng. Rehabil.*, vol. 14, no. 1, pp. 1–12, 2017.

[40] N. de la Oliva, J. del Valle, I. Delgado-Martínez, M. Mueller, T. Stieglitz, and X. Navarro, "Long-term functionality of transversal intraneural electrodes is improved by Dexamethasone treatment," *IEEE Trans. Neural Syst. Rehabil. Eng.*, vol. 27, no. 3, pp. 457–464, Oct. 2019.

[41] C. Hassler, T. Boretius, and T. Stieglitz, "Polymers for neural implants," *J. Polym. Sci. B, Polym. Phys.*, vol. 49, no. 1, pp. 18–33, Jan. 2011.

[42] T. Stieglitz, H. Beutel, M. Schuettler, and J. U. Meyer, "Micromachined, polyimide-based devices for flexible neural interfaces," *Biomed. Microdevices*, vol. 2, no. 4, pp. 283–294, 2000.

[43] C. J. Bettinger, "Recent advances in materials and flexible electronics for peripheral nerve interfaces," *Bioelectronic Med.*, vol. 4, no. 1, pp. 1–10, Dec. 2018.

[44] Z. Xiang *et al.*, "Progress of flexible electronics in neural interfacing—A self-adaptive non-invasive neural ribbon electrode for small nerves recording," *Adv. Mater.*, vol. 28, no. 22, pp. 4472–4479, Jun. 2016.

[45] S. Lee *et al.*, "Toward bioelectronic medicine-neuromodulation of small peripheral nerves using flexible neural clip," *Adv. Sci.*, vol. 4, no. 11, Nov. 2017, Art. no. 1700149.

[46] S. Lee, Q. Shi, and C. Lee, "From flexible electronics technology in the era of IoT and artificial intelligence toward future implanted body sensor networks," *APL Mater.*, vol. 7, no. 3, Mar. 2019, Art. no. 031302.

[47] J. Badia *et al.*, "Selectivity of the TIME implantable nerve electrode," in *Direct Nerve Stimulation for Induction of Sensation and Treatment of Phantom Limb Pain* (River Publishers Series in Biomedical Engineering). Gistrup, Denmark: River Publishers, 2019, pp. 171–191.

[48] L. A. Geddes and R. Roeder, "Criteria for the selection of materials for implanted electrodes," *Ann. Biomed. Eng.*, vol. 31, no. 7, pp. 879–890, Jul. 2003.

[49] K. M. Szostak, L. Grand, and T. G. Constandinou, "Neural interfaces for intracortical recording: Requirements, fabrication methods, and characteristics," *Frontiers Neurosci.*, vol. 11, p. 665, Dec. 2017.

[50] S. F. Cogan, "Neural stimulation and recording electrodes," *Annu. Rev. Biomed. Eng.*, vol. 10, no. 1, pp. 275–309, Aug. 2008.

[51] R. Atmaramani *et al.*, "Ruthenium oxide based microelectrode arrays for *in vitro* and *in vivo* neural recording and stimulation," *Acta Biomaterialia*, vol. 101, pp. 565–574, Jan. 2020.

[52] E. Cuttaz *et al.*, "Conductive elastomer composites for fully polymeric, flexible bioelectronics," *Biomater. Sci.*, vol. 7, no. 4, pp. 1372–1385, 2019.

[53] E. Brunton, C. W. Blau, and K. Nazarpour, "Separability of neural responses to standardised mechanical stimulation of limbs," *Sci. Rep.*, vol. 7, no. 1, Dec. 2017, Art. no. 11138.

[54] H. Schmalbruch, "Fiber composition of the rat sciatic nerve," *Anatomical Rec.*, vol. 215, no. 1, pp. 71–81, May 1986.

[55] B. Katz and R. Miledi, "The measurment of the dynaptic delay and the time course of acetylcholine release at the neuromuscular junction," *Proc. Roy. Soc. B, Biol. Sci.*, vol. 161, pp. 483–495, Oct. 1965.

[56] C. Veraart, W. M. Grill, and J. T. Mortimer, "Selective control of muscle activation with a multipolar nerve cuff electrode," *IEEE Trans. Biomed. Eng.*, vol. 40, no. 7, pp. 640–653, Jul. 1993.

[57] N. de la Oliva, M. Mueller, T. Stieglitz, X. Navarro, and J. del Valle, "On the use of Parylene C polymer as substrate for peripheral nerve electrodes," *Sci. Rep.*, vol. 8, no. 1, Dec. 2018, Art. no. 5965.

[58] S. Wurth *et al.*, "Long-term usability and bio-integration of polyimide-based intra-neural stimulating electrodes," *Biomaterials*, vol. 122, pp. 114–129, Apr. 2017.

[59] R. Caldwell, M. G. Street, R. Sharma, P. Takmakov, B. Baker, and L. Rieth, "Characterization of Parylene-C degradation mechanisms: *In vitro* reactive accelerated aging model compared to multiyear *in vivo* implantation," *Biomaterials*, vol. 232, Feb. 2020, Art. no. 119731.

[60] A. Prasad *et al.*, "Comprehensive characterization and failure modes of tungsten microwire arrays in chronic neural implants," *J. Neural Eng.*, vol. 9, no. 5, Oct. 2012, Art. no. 056015.

[61] J. C. Williams, J. A. Hippensteel, J. Dilgen, W. Shain, and D. R. Kipke, "Complex impedance spectroscopy for monitoring tissue responses to inserted neural implants," *J. Neural Eng.*, vol. 4, no. 4, pp. 410–423, Dec. 2007.

[62] T. Stieglitz and J.-U. Meyer, "Biomedical microdevices for neural implants," in *Proc. BioMEMS*, 2006, pp. 72–137.

[63] K. C. Cheung, "Implantable microscale neural interfaces," *Biomed. Microdevices*, vol. 9, no. 6, pp. 923–938, Oct. 2007.

[64] H. S. Sohal *et al.*, "The sinusoidal probe: A new approach to improve electrode longevity," *Frontiers Neuroeng.*, vol. 7, p. 10, Apr. 2014.